Modelling the upper yield point and the brittle-ductile transition of silicon wafers in three-point bend tests

Steve G Roberts, Peter B Hirsch

Modelling the upper yield point and the brittle-ductile transition of silicon wafers in three-point bend tests

Journal:	*Philosophical Magazine & Philosophical Magazine Letters*
Manuscript ID:	TPHM-05-Sep-0413.R1
Journal Selection:	Philosophical Magazine
Date Submitted by the Author:	08-Feb-2006
Complete List of Authors:	Roberts, Steve; University of Oxford, Materials Science Hirsch, Peter; University of Oxford, Materials
Keywords:	modelling, brittle-ductile transition, crystals, deformation, dislocations, fracture, dislocation dynamics, dislocation mechanics
Keywords (user supplied):	

Nabarro Festschrift
Submitted to Phil. Mag, Sept 2005
Revised version Feb. 2006

Modelling the upper yield point and the brittle-ductile transition of silicon wafers in three-point bend tests

S.G. Roberts and P.B. Hirsch

Department of Materials, University of Oxford,
Parks Road, Oxford, OX1 3PH

Abstract

Three point bend test carried out by Folk[1] on initially dislocation-free specimens of semiconductor-grade single crystals of Si showed that, for a given strain-rate, above a critical temperature, T_c, and at a certain stress, a large load drop occurs upon yielding and the sample deforms plastically. Below T_c specimens fail by brittle fracture after a small load drop, or at even lower temperatures without apparent prior plastic flow. This paper describes a simple dislocation model and computer simulation to explain the occurrence of a yield drop, the strain-rate dependence of T_c and Folk's etch pit observations of the plastic zone. Good agreement is obtained between the temperature dependence of the upper yield stress and the strain-rate dependence of T_c with the predictions of the model. These parameters are controlled by dislocation velocity.

Dedication

This paper is dedicated to Frank Nabarro in honour of his 90th birthday. He has made many outstanding and lasting contributions to dislocation theory,

and has championed the application of quantitative analysis in crystal plasticity.

1. Introduction

The brittle-ductile transition (BDT) in silicon has been studied extensively over the last thirty years, with most experiments conducted on precracked specimens [2-7]. The observed transitions are sharp and the activation energy controlling the strain-rate dependence of the transition temperature (T_c) was found to be close to that controlling dislocation velocity (for reviews see [8,9]). The intercepts of the Arrhenius plots however vary greatly depending on the test geometry, crystal growth technique, procedure of introducing the crack, and composition. This suggests that although the temperature dependence in all cases is controlled by dislocation velocity, T_c at any given strain-rate is structure sensitive. Two different models were suggested, applicable to different geometries, in which the critical event in a constant strain-rate test is the nucleation of crack tip sources, which, in the high stress field near the crack tip, rapidly emit avalanches of dislocations sufficient to shield the crack completely before the applied stress intensity factor reaches K_{IC} for brittle fracture [8,9]. In these models it is the nucleation of crack tip sources by gliding dislocations which controls the strain-rate dependence of T_c. The structure sensitivity of T_c is simply due to the different distances the dislocations have to move either to the crack or along the crack to generate these sources. Each intercept in the Arrhenius plots corresponds to a characteristic distance the dislocations have to move to nucleate the

sources. These models are supported by experiment and computer simulation [8,9]. The remarkable sharpness of the transition in crystals with few initial dislocations is attributed to the sources, once nucleated, being highly stressed for dislocation emission.

Khantha, Pope and Vitek [10] put forward a theory for the BDT in which a critical combination of stress and temperature results in the massive generation of dislocations arising from a cooperative Kosterlitz-Thouless type instability [11], permitting general yielding. No crack tip is necessary for this transition. To test this hypothesis Folk [1] carried out three point bend tests on initially dislocation-free specimens of single crystals of Si. No precracks were intentionally introduced into the specimens, which were produced from Si wafers using photolithography. The experiments revealed that, for a given strain-rate, above a critical temperature (the BDT temperature T_c) and at a certain stress, a large load drop occurs upon yielding and the sample begins to flow. Below this temperature the sample fails by brittle fracture, at a stress σ_F which is strongly temperature dependent, either without apparent prior plastic flow, or, near the critical temperature (within 10-50° of T_c), after some plastic flow which causes deviation from linearity in the load-displacement curve, and/or a small yield drop. Figure 1 shows the three types of behaviour. The lowest temperature transition from type 2 to type 3 defines T_c. However some specimens exhibit type 2 behaviour up to 30° above T_c. T_c is found to be strain-rate dependent, with an activation energy (1.9 ev) close to that for dislocation velocity. Etch pit observations carried out after unloading show the development of a plastic zone under the knife edge loading probe before

the critical stress at T_c is reached. No detailed interpretation of the nature and development of the plastic zone, of the strain-rate dependence of T_c, and of the temperature dependence of the fracture stress σ_F have been published, but it is claimed that the BDT is not controlled by dislocation velocity [1,12] and that the behaviour is qualitatively consistent with the Khantha, Pope and Vitek model [10].

The object of the present paper is to explain the observations of the plastic zone, the occurrence of a yield drop, and the strain-rate dependence of T_c. The following sections (2, 3, 4) give first a brief summary of the salient features of Folk's results, secondly a description of a simple model to explain the observations, and thirdly, a computer simulation to explain the occurrence of a yield drop and to determine the temperature dependence of the upper yield stress, the strain-rate dependence of T_c, and the etch pit observations. Section 5 discusses the temperature dependence of σ_F, and the final section compares the model with previous models for the BDT in precracked specimens.

2. Summary of Folk's (2000) main results

Fig. 1 illustrates the three types of behaviour observed: brittle, brittle with some prior plasticity, and fully plastic. Fig. 2 shows schematically the experimental arrangement. Fig. 3 shows the maximum bending stress against temperature for a strain-rate of 6×10^{-5} s^{-1}. The results for different strain-rates are similar. According to Folk (2000), between room temperature and about 900K the fracture is purely brittle with no

observable macroscopic deformation (type I behaviour) and the fracture stress, σ_F, varies widely between specimens from different wafers, and less widely between specimens from a given wafer. In this temperature range σ_F varies between about 1.5GPa and 3.5GPa, indicated in fig. 3 by the dashed horizontal lines. Above about 900K, the brittle fracture stress, σ_F, is strongly temperature dependent. T_c is defined as the lowest temperature at which the specimen becomes ductile. The strain-rates $\dot{\varepsilon}$ used in the experiments were $6x10^{-6}$ s^{-1}, $3x10^{-5}$ s^{-1}, $6x10^{-5}$ s^{-1}, $1.2x10^{-4}$ s^{-1} and $6x10^{-4}$ s^{-1}. A plot of ln $\dot{\varepsilon}$ against T_c^{-1} is consistent with an activation energy for T_c of 1.9ev. The applied maximum bending stress, i.e. the upper yield stress, at which T_c occurs is found to vary slightly; the values are 802 MPa, 841 MPa, 843 MPa, 765 MPa for the first four strain-rates listed above. For the highest strain-rate, $6x10^{-4}$ s^{-1}, the specimens failed in a brittle manner at all temperatures at which tests were made, up to 1246K.

Etch pit observations were made with the SEM on samples tested with $\dot{\varepsilon}=6X10^{-5}$ s^{-1} at 967K and 979K, just below and above T_c=972K, unloaded at various stages. The images cover the inclined side walls of the beam as well as part of the tensile surface. Fig. 4 shows the etch pit distributions for the specimens tested at 979K, unloaded at a) 60%, b) 80% c) 100% of the peak stress, d) after the load drop. The pictures corresponding to a, b, c for the sample tested at 967K are qualitatively similar to those tested at 979K. It should be noted that the etch pit distributions show the dislocation arrangements after unloading, not in the loaded state (see section 4).

3. A model for the occurrence of a load drop

The etch pit observations made by Folk [1] just above and below T_c show that there are essentially three types of dislocation activity:-

I) Shear bands parallel to (111) and $(\bar{1}\bar{1}1)$ (the "primary" system) generated by dislocation emission at the edges of the central loading contact. Some of these dislocations travel across the specimen and reach the tensile surface in the loading/unloading cycle at stresses as low as 60% of the upper yield stress.

II) Slip traces parallel to [110], corresponding to slip activity on the $(\bar{1}11)$, $(1\bar{1}1)$ ("cross-slip") systems. The development of these slip lines lags behind those of the primary systems and they do not reach the tensile surface (after unloading) till the stresses approach the upper yield point.

III) Strong slip lines on the primary systems activated at the upper yield point, which are nucleated in the tensile section of the beam, or at the tensile surface.

We suggest the following sequence of events (see figure 5):-

1) The initial shear bands, I, on (111) and $(\bar{1}\bar{1}1)$ are generated at the edges of the loading contact, which acts approximately as a flat punch. The shear stress on these systems is maximum at these locations [13]. The extra half planes of the dislocations lie above the slip planes as shown in fig. 5a. The signs of these dislocations are such that the compressive bending stress, which acts on the loading probe side of the beam aids the generation of these dislocations, but the dislocations do not relieve the stresses on the tensile side of the bent beam. In fact they are repelled by the tensile stress (fiig. 5b) and

increase the surface tensile stress (see section 5). The passage of these dislocations across the neutral axis is primarily due to their mutual interaction.

2) The stress on system II from the loading knife edge, and close to it, is largely hydrostatic compression with a smaller tensile component parallel to the length of the punch [13]. The early development of these slip systems will therefore lag behind that of system I. However the dislocations on system I exert a compressive stress along [001] (fig 5b: σ_{disln}), which aids the development of the dislocations on system II, which will accelerate as the dislocations on I accumulate (fig 5c).

3) Eventually these cross-slip dislocations will reach the tensile surface. Since the dislocations in Si are dissociated into Shockley partials, for any screw dislocation intersecting the surface these partials will either constrict or expand depending on their sign [14]. Those which constrict can cross-slip readily (onto the (111) and ($\overline{1}\overline{1}1$) planes of system I) (figs. 5c, 5d), forming single ended Frank-Read sources. These will operate rapidly in the highly stressed surface regions of the beam, producing avalanches of dislocations (system III) on slip planes containing the sources (see fig. 5e), which produces a yield drop. The fact that system III slip consists of a series of slip bands is consistent with the operation of Frank-Read sources. The sign of these dislocations is the same as for system I, but they are moving in the opposite direction, from the tensile surface to the neutral axis.

Fig. 6 shows a computer simulation for a strain-rate $\dot{\varepsilon}=6\text{x}10^{-5}$ s^{-1} at $T_c=972K$ of the number of dislocations generated and the array length on a

single type III slip plane, following nucleation of one source at the tensile surface, at two stresses just below that at which T_c occurs. This emphasizes the large number of dislocations produced very rapidly by one Frank-Read source. Each slip band contributes a yield drop. With increasing numbers of sources operating at the same time the yield drop increases resulting finally in plastic flow at a low stress. No mechanism other than the operation of Frank-Read sources is required.

The condition for obtaining a yield drop is that the dislocations on the cross-slip plane reach the tensile surface and generate Frank-Read sources on system III before fracture occurs. This means that the yield drop condition and the upper yield stress are controlled by dislocation velocity. In the next section we describe a model for this which gives the upper yield stress as a function of temperature and strain-rate. Experimentally, T_c is found to occur at an upper yield stress of about 800MPa at various strain-rates, and the model for the upper yield stress is then used to determine the strain-rate dependence of T_c.

The change from elastic to fully plastic deformation in this case is interesting. System I is activated first through the action of the loading probe. Slip on this system reduces the bending stress in the compressive part of the bent beam. But system I is repelled by the tensile part of the beam which is still deforming elastically. When system III is activated, the tensile stress decreases; this enables system I to develop further reducing the compressive bending stress. Unless brittle fracture intervenes, this process continues until most of the strain-rate can be accommodated by

plastic flow both in the "tensile" and "compressive" parts of the beam. System I transports material away from the compressive side of the beam; system III extends the tensile part of the beam plastically. These two systems effectively act to produce a plastic hinge. System II acts as the agent which initiates slip on system III. In addition there is accommodating convergent slip under the finite width loading contact.

4. Modelling the upper yield stress and the strain-rate dependence of T_c

We assume that the loading contact acts as a long flat punch, subject to a uniform pressure P. The punch stress field σ_P is given by Nadai [15] as

$$\left.\begin{aligned}
\sigma_{xx} &= -\frac{P}{2\pi}\left[2(\theta_1-\theta_2)+\sin 2\theta_1-\sin 2\theta_2\right]\\
\sigma_{yy} &= -\frac{P}{2\pi}\left[2(\theta_1-\theta_2)-\sin 2\theta_1+\sin 2\theta_2\right]\\
\tau_{xy} &= \frac{P}{2\pi}(\cos 2\theta_1-\cos 2\theta_2)\\
\sigma_{zz} &= \upsilon(\sigma_{xx}+\sigma_{yy})
\end{aligned}\right\} 1$$

The coordinates and angles are shown in fig. 5f; υ is Poisson's ratio. The diverging slip lines on system I are generated at the edges of the punch where the shear stress is a maximum, as shown in fig. 5. These stresses, together with the applied bending stress σ_B, are used to calculate the resolved shear stresses on dislocations on the (111) and $(\bar{1}\bar{1}1)$ planes of system I. Each of the diverging shear bands are treated as slip on single planes. To simplify the calculation the two sets of dislocations on each plane (e.g. ½$[\bar{1}01]$ and ½$[0\bar{1}1]$ on (111)) are replaced by one edge

dislocation (b along $[\bar{1}\bar{1}2]$). The dislocations on the $(\bar{1}11)$, $(1\bar{1}1)$ planes of system II are treated in the same way; i.e. dislocations with $b=\frac{1}{2}[0\bar{1}1]$ and $b=\frac{1}{2}[101]$ on $(\bar{1}11)$ are replaced by pure edge dislocations with b along $[1\bar{1}2]$. The stresses acting on these dislocations are σ_P and the interaction stresses from system I. For simplicity the interaction between them is calculated as that of an infinite straight dislocation on I on the midpoint of a dislocation on II. (The reverse interaction is neglected because the number of dislocations on a single slip plane on I is much greater than that on II). Interaction between the dislocations moving on the same planes is fully taken into account (assuming them to be infinitely long), as is that between dislocations on the two shear bands on system I. Although the etch pit distribution on the inclined face (see fig. 4) shows slip on system II to occur on planes a few microns apart, this has been modelled as slip on a single plane. A previous comparison between dislocations moving on a single slip plane, and several parallel slip planes, in a crack tip stress field showed the use of the single slip plane model to be a reasonable approximation [16]. Furthermore, the length of a single slip line representing the plastic zone at a semi-infinite crack is found to be within about 5% of that predicted by the finite element model [17]. The bend stresses are calculated for the trapezoidal beam shown in fig. 2. P is calculated from the beam deflections by assuming a punch width ω of 50μm; in practice the etch pit observations of the distance between the initiation locations of the shear bands show this to be somewhat variable (see fig. 4 and [1] for other examples), but the above value appears representative. (A simulation carried out for ω=70μm, gives essentially the same results for ω=50μm). The dislocation velocity is given by

$$v = v_0 \left| \frac{\tau}{\tau_0} \right|^m \exp\left(-\frac{U}{kT} \right) \quad (2)$$

For intrinsic Si, v_0=1.8x10^5 ms^{-1}, τ_0=19 MPa, m=1.6, U=2.22 eV [18]; τ is the shear stress acting on the dislocations. For the calculation of the interaction stresses the shear modulus μ=62 GPa, b=0.381 nm, ν =0.218.

In the calculation dislocation sources are assumed to be situated at b from the punch face along the slip plane. (The results of the simulations are insensitive to the distance of the source from the punch face for values ranging from b to 100b). Each emitted dislocation moves away from the source according to equation (2), and when the total stress at the source becomes positive a further dislocation is emitted. The applied stress increases at a constant rate determined by the strain-rate. This dynamic simulation model is similar to that used previously in treating emission from loaded crack tips (e.g. [8]), except that the stress fields here are different.

Fig. 7 shows the results of the simulation for $\dot{\varepsilon}$=6x10^{-5} s^{-1} at 972K, the experimental T_c for this strain-rate. The figure shows the length of the slip lines and the total number of dislocations on systems I and II as a function of bend stress. System I develops initially more quickly than system II, reaching the neutral axis (~175 μm along the slip plane) at a much lower stress than system II. But then system II catches up and reaches the surface at 800MPa, while system I does not. The comparison with the etch pit results is not straightforward, since the latter observations are made on unloaded specimens above and below T_c (see fig. 4), while the predictions in fig. 7 correspond to the loaded state at T_c. Simulations in which the

loaded specimens above and below T_c are unloaded at the temperature at which loading occurred, show that unloading allows the arrays to move further. The dislocations on system I, in particular, expand rapidly towards the tensile surface, since unloading reduces and then removes the bend stress which opposes their motion near the tensile surface. Unfortunately the thermal history of Folk's unloading experiments is not known, and so no detailed comparisons are possible. Nevertheless, the etch pit results in fig. 4 and others in Folk's thesis are consistent with the proposed model that nucleation of many new slip lines at the tensile surface occurs when the system II dislocations reach the surface. On the other hand the etch pit results show that the primary dislocations seem to reach the tensile surface before the "cross-slip" dislocations, while this is not the case in the computer simulation. This may be partly due to unloading effects, but simulations carried out in which the back interaction from system II to system I is taken into account in an approximate way, show that this has the effect of speeding up the progress of the system I dislocations, but we cannot be certain whether they meet the surface before system II.

The curves obtained at the other strain-rates and experimentally observed values of T_c are very similar to fig. 7. Fig. 8 plots the temperature at which system II reaches the surface (initiating nucleation of sources on system III) against the maximum bending stress (the upper yield stress) for $\dot{\varepsilon}=6\text{x}10^{-5}\ s^{-1}$. The experimental values of the upper yield stress are also shown. The agreement between the model predictions and the experimental values of the upper yield stress is good, and the same is true for the other strain-rates, providing support for the dislocation velocity

controlled nucleation model. At the stress at which T_c is observed experimentally (~800 MPa), the predicted T_c is 967K (compared with 972K observed experimentally). The predicted values of T_c for the other strain-rates are obtained in the same way, and are compared with experiments in table 1. Fig. 9 plots ln(strain-rate) against T_c^{-1} for the model and for the experiment. The agreement is excellent. It should be noted that while the computer modelling includes several simplifications, there are no adjustable parameters in the calculation.

It should be noted however that while this model explains the mechanism by which dislocation sources are nucleated to produce a yield drop, and while it predicts correctly the temperature dependence of the upper yield stress, and T_c at the experimentally observed stress, it does not explain why the BDT occurs at these particular stresses. To do this, we need to understand the origin of the fracture stress.

5. The temperature dependent brittle fracture stress

According to Folk [1], at low temperatures (~725K – 900K) the fracture is purely brittle and σ_F varies between about 1.5GPa and 3.5GPa, similar to the range observed at room temperature. Above this temperature the maximum bending stress is strongly temperature dependent. Fig. 3 shows the observed maximum bending stress at fracture σ_F against temperature for $\dot{\varepsilon}=6\text{x}10^{-5}$ s^{-1}. The fracture stress at this strain-rate drops in the high temperature regime from 1GPa at 936K to about 0.4GPa at 1004K. Such a rapid decrease with temperature is likely to be caused by dislocation

activity. Furthermore, the scatter of σ_F above about 900K in Folk's results at different strain-rates is surprisingly low, suggesting that the controlling flaw above this temperature is generated by the deformation.

The most likely site for crack initiation is probably at a stress concentrator at the tensile surface, such as a step or notch produced by slip lines on system III nucleated where cross-slip dislocations meet the surface. The fact that fracture takes place at stresses σ_F slightly lower than the upper yield stress, suggests that for cracking to occur slip steps on system III have to be formed, i.e. that σ_N is reached. The variation of σ_F with temperature will then be similar to that of σ_N, but the stresses will be slightly lower because of the load drop. This explains the observed variation of σ_F with temperature. Fig. 8 shows the experimental values of σ_F (diamonds) as a function of temperature. Most of the points lie below σ_N, and follow the same temperature variation.

Slip on system III takes place on two planes, (111) and $(\overline{1}\overline{1}1)$. If slip on both planes occurs near the same location on the surface, and with the two {111} slip steps facing each other, a V notch with semi angle 35° is produced. Fig. 6 shows that if slip takes place on single slip planes at the fracture stress, σ_F, large steps, of the order of 1μm high can be generated in a short time. The tensile stress at the tip of the notch is $2\sigma_F(a/\rho)^{1/2}$ where a is the height of the slip step and ρ is the radius of curvature at the root of the notch. With a~1μm and ρ of nanometre dimensions, stresses ~ $50\sigma_F$ can occur at the root of the notch, sufficient to nucleate cracking. Alternatively the root may already be cracked if the slip steps occur at an

existing flaw (see below). Treating the combined notch and microcrack as a crack of length a, crack propagation could be expected at a stress of approximately $K_{IC}/(\pi a)^{1/2}$, where K_{IC} is the fracture toughness of silicon (1MPa $m^{1/2}$), i.e. about 560MPa for a=1μm, less than the observed σ_F at T_c. Thus notches of this type (some bigger, some smaller) can cause fracture of the specimen at the observed fracture stresses. We suggest therefore that the flaws controlling fracture may be pairs of slip steps forming sharp V notches. However, if the slip is diffuse, e.g. if the slip lines broaden by double cross-slip, the resulting U notch will have a larger radius of curvature, be less potent , and may not be able to cause cracking. It may be noted that there are examples on Folk's micrographs of slip lines on the (111) and $(\overline{1}\overline{1}1)$ planes appearing, albeit on low resolution, to come from the same location on the surface (see figs. 4c, d).

Whether fracture or plastic flow occurs depends on the number of sources nucleated at the same time and on the size of the slip steps. If only a few sources are nucleated at a given time when the cross-slip dislocations meet the surface and the slip lines do not broaden, the load drop will be too small and fracture will be favoured, but when many sources are nucleated and the slip lines broaden by double cross-slip, the load drop can be sufficient (and the slip steps less potent) for fracture to be inhibited and plastic flow to occur. Since the formation of a source by cross-slip is likely to involve some thermally activated process, and the same will be true for broadening of slip lines by double cross-slip, higher temperature is likely to favour a large yield drop. Thus in fig. 8, within the range at which an upper yield point is observed, below T_c only a few sources are nucleated, forming sharp

slip steps, and above T_c the rate of nucleation and broadening by cross-slip increases until no reversion to fracture occurs. To determine the bend stress at which plastic flow, i.e. T_c, occurs, we need to model the load drop in terms of the number of sources nucleated at σ_N, their rate of emission of dislocations and the slip line broadening as the load decreases. This is not included in the present model and remains to be done. In this paper we therefore determine T_c by assuming the experimentally observed value of σ_F at the transition (see section 4).

At the highest strain-rate of $6x10^{-4}$ s^{-1} no transition occurs experimentally and the specimens fail by brittle fracture even at the highest temperature investigated (1246K). Fig. 10 shows the experimental values of the upper yield stress and fracture stress as a function of temperature for this strain-rate [1], and the curve of σ_N predicted by the model. The agreement in this case is again good, particularly above 950K, and a transition might be expected in this temperature range. The brittle behaviour may be due to a paucity of sources and large slip steps at the high strain-rate, but this requires further investigation by modelling the rate of nucleation and the broadening of the slip lines.

Fig. 10 also shows that at this strain-rate between ~900K and 1000K, brittle fracture occurs without any observable macroscopic deformation at values of σ_F which decrease sharply with increasing temperature, at a rate similar to, but somewhat below, σ_N determined by the model. The fact that plasticity cannot be observed on the stress-strain curves does not exclude the possibility of some plastic flow occurring. The reason for the

discrepancy between the predicted σ_F and observed values of σ_N is not clear. Below 900K the fracture is assumed to be controlled by pre-existing flaws in the specimen; at a mid-range stress of 2.5GPa the typical flaw size is ~50nm. At the lower strain-rates there are only 2 or 3 such datapoints at each strain-rate. At each strain-rate (except for the highest, see fig. 10) the fracture stresses, which fall within the same range as those at room temperature, are highest at the lowest temperature, down to about 725K (see e.g. fig. 3), but the data are too sparse to attempt any meaningful analysis.

6. Discussion

The conditions for the occurrence of a BDT in Folk's experiments have some similarities with those which control the BDT in precracked specimens. In Folk's experiments the plastic zone on system III in the tensile part of the beam has to be developed rapidly to cause a sufficiently large load drop to prevent brittle fracture. In the precracked specimen the crack has to be shielded before the applied stress reaches the value needed to cause brittle fracture. In both cases the plasticity is brought about by dislocation avalanches produced by new sources nucleated by the motion of dislocations either to the surface (present experiments) or to or along the precrack [8,9]. As in the case of precracked specimens the nucleation of the sources is controlled by dislocation velocity, and in both cases the dislocations move a distance characteristic of the experimental and specimen conditions, resulting in "structure sensitivity" of the BDT. In both

cases it is this process which causes the strain-rate dependence of T_c to be controlled by dislocation velocity.

There are however some important differences. Firstly, in the present experiments the brittle fracture stress σ_F is strongly temperature dependent, whereas for the precracked specimens brittle fracture occurs at the precrack at K_{IC} which is relatively temperature independent. The reason for this strong temperature dependence is that in this case the critical surface flaws are nucleated by the dislocation activity itself, and the temperature dependence of σ_F follows that for nucleation of surface sources by cross-slip, i.e. σ_N. Unlike the case of bend tests on precracked specimens, in most cases fracture actually occurs after a small load drop, due to the formation of stress relieving slip lines. Whether fracture or plastic hinging occurs after the sources are nucleated on system III depends critically on whether only a few dislocation sources are nucleated which provide insufficient slip to relieve the tensile stress before fracture occurs, and which form sharp slip steps acting as potent notches, or whether many sources are nucleated, the slip steps are gradual and the notches are less potent, in which case plastic flow occurs. The attainment of this latter condition determines T_c. Secondly, the range of temperatures in which it is uncertain whether flow or fracture occurs can be as much as 30°, compared to less than 5° for precracked undeformed Si (e.g. [4]). Thirdly, at a high strain-rate brittle fracture occurs at all temperatures investigated, including temperatures much higher than that at which T_c might be expected. This is quite different from the situation for precracked

specimens, where a BDT is observed and expected at all the strain-rates used in the experiments.

Acknowledgements

We are grateful to Professor David Pope for sending us a copy of Folk's thesis, and to Professor Vaçek Vitek for emailing copies of the micrographs. We would like to pay tribute to Dr. Folk for his excellent experimental study. Our thanks are also due to Professor G. D. W. Smith for providing laboratory facilities.

References

1 R.H. Folk, The Brittle to Ductile Transition in Silicon: Evidence of a Critical Yield Event, Ph.D. thesis, University of Pennsylvania (2000).
2 C. St. John, Phil. Mag. **32** 1193 (1975).
3 K. Brede and P. Haasen, Acta Metall. **36** 2003 (1988).
4 J. Samuels and S.G. Roberts, Proc. R. Soc. Lond. **A421** 1 (1989).
5 H. Azzouzi, G. Michot and A. George, Proc. 9th Conf. on Strength of Metals and Alloys, edited by D.G. Brandon, R. Chaim and A. Rosen (Freund: London, 1991) pp. 783-789.
6 A. George and G. Michot, Mater. Sci. Engin. **A164** 118 (1993).
7 B.J. Gally and A.S. Argon, Phil. Mag. **81** 699 (2001).
8 P.B. Hirsch and S.G. Roberts, Phil. Mag. **64** 55 (1991).
9 P.B. Hirsch and S.G. Roberts, Acta Mater. **44** 2361 (1996).
10 M. Khantha, D.P. Pope and V. Vitek, Scripta Metall. Mater. **31** 1349 (1994).
11 J.M. Kosterlitz and D.J. Thouless, J. Phys. C: Solid State Phys. **6** 1181 (1973).
12 R.H. Folk, M. Khantha, D.P. Pope and V. Vitek, MRS Proceedings **539**: Fracture and Ductile vs. Brittle Behavior - Theory, Modeling, and Experiment, edited by G.E. Beltz, R.L. Blumberg Selinger, K.-S. Kim, and M.P. Marder (Materials Research Society, Warrendale, PA, USA, 1999) pp. 161-167.
13 S.G. Roberts, P.D. Warren and P.B. Hirsch, J. Mater. Res. **1** 162 (1986).
14 P.M. Hazzledine, Fundamentals of Deformation and Fracture, edited by B.A. Bilby, K.J. Miller, and J.R. Willis (Cambridge University Press: Cambridge, 1985), p. 385.
15 A. Nadai, Plasticity (McGraw-Hill, New York, 1931), p. 247.
16 S.N. Noronha, S.G. Roberts and A.J. Wilkinson, MRS Proceedings **578**, Multiscale Phenomena in Materials – experiments and modelling, edited by I.M. Robertson, D.H. Lasila, B. Devincre and R. Phillips (Materials Research Society, Warrendale, PA, USA, 2000), pp. 309-314.
17 P.B. Hirsch and S.G. Roberts, Phil. Trans. R. Soc. Lond. **A355** 1991 (1997).
18 A. George and G. Champier, Phys. Stat. Sol. **53a** 529 (1979).

Nabarro Festschrift
Submitted to Phil. Mag, Sept 2005
Revised version Feb. 2006

Table 1

Experimental and modelled brittle – ductile transition temperatures

	Brittle – ductile transition temperature (K)	
Strain rate (s^{-1})	Experiment	Model
6.0×10^{-6}	885	890
3.0×10^{-5}	938	943
6.0×10^{-3}	972	967
1.2×10^{-4}	1006	994
6.0×10^{-4}	No Transition	1066

Figure Captions

Figure 1: Typical stress –strain curves for 3-point bending tests on silicon beams at temperatures around the brittle-ductile transition: type1 - brittle (727K); type 2 - brittle with prior plasticity (1003K); type 3 - fully plastic (1006K).

Figure 2: Geometry and crystallographic orientation of silicon three-point bend specimens used by Folk (2000) for brittle-ductile transition experiments.

Figure 3: Typical experimental results (Folk 2000); fracture, upper yield and flow stresses as a function of test temperature for a strain rate of 6×10^{-5} s^{-1}. The dashed lines indicate the upper and lower limits of low temperature brittle fracture stresses.

Figure 4: SEM micrographs of the etched inclined side and tensile faces of specimens loaded at 6×10^{-5} s^{-1} and 979K to (a) 60%, (b) 80% and (c) 100% of the peak stress, and (d) after the load drop. The central loading contact is on the bottom edge in each case.

Figure 5: Proposed sequence of dislocation motion in the tests (see text): a) dislocations on type I slip systems nucleate at the contact edges and glide towards the tensile side of the specimen; b) secondary slip systems (type II) operate under the stresses from the contact and from dislocations on the primary systems; c) primary and secondary dislocations approach the tensile surface; d) secondary dislocation emerges at the tensile surface leaving a screw segment; e) screw segment cross-slips onto primary slip system forming a source near the tensile surface which can rapidly generate dislocations of type III; f) Dislocation types used in the model; co-ordinates used in equations (1) are also shown. For clarity, in (a)-(e), only one geometric variant of each slip system is shown, and the junctions between dislocations on type II and type I systems which terminate the type II dislocations are not shown.

Figure 6: Modelling of type III dislocation arrays, nucleated at the tensile surface at two levels of bend stress (750 and 790 MPa). Strain rate = 6×10^{-5} s^{-1}, temperature = T_c for this strain rate = 972K. Fracture stress at the BDT is ~800 MPa (vertical dotted line).

Figure 7: Modelling of types I and II dislocation arrays. Strain rate = 6×10^{-5} s^{-1}, temperature = T_c for this strain rate = 972K. Fracture stress at the BDT is ~800 MPa (vertical dotted line). Horizontal dotted lines indicate the dislocation array lengths corresponding to the specimen's neutral axis and tensile surface.

Figure 8: Temperature dependence of experimental fracture stress and experimental and modelled yield stress at a strain rate of 6×10^{-5} s^{-1}. The horizontal dotted line indicates the average experimental fracture stress at the brittle-ductile transition (800MPa); vertical lines indicate the experimental T_c (972 K) and the modelled T_c, where the modelled yield stress equals 800 MPa (967K).

Figure 9: Arrhenius plots of strain-rate dependence of experimental and modelled brittle ductile transition temperatures (T_c). Activation energies corresponding to the best-fit lines are 1.9 eV for the experimental data and 2.2 eV for the model.

Figure 10: Experimental results (Folk 2000) for a strain rate of 6×10^{-4} s^{-1}; fracture and upper yield as a function of test temperature. The results of the model for upper yield stress (σ_N) for the same conditions are also shown..

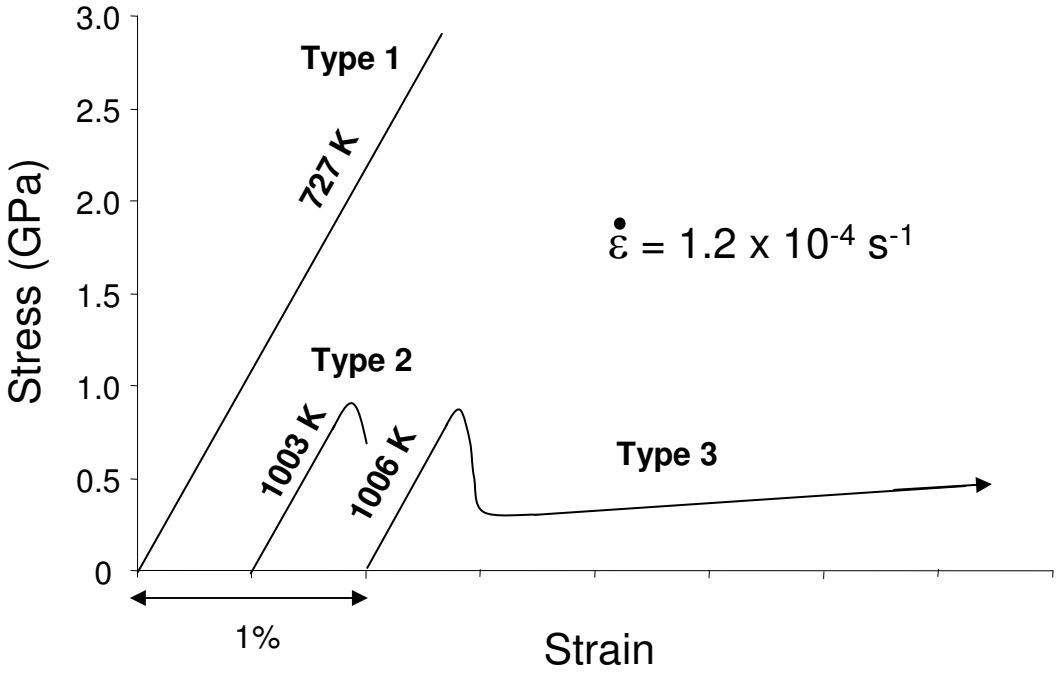

Figure 1: Typical stress-strain curves for 3-point bending tests on silicon beams at temperatures around the brittle-ductile transition: type1 - brittle (727K); type 2 - brittle with prior plasticity (1003K); type 3 - fully plastic (1006K).

Fig. 1

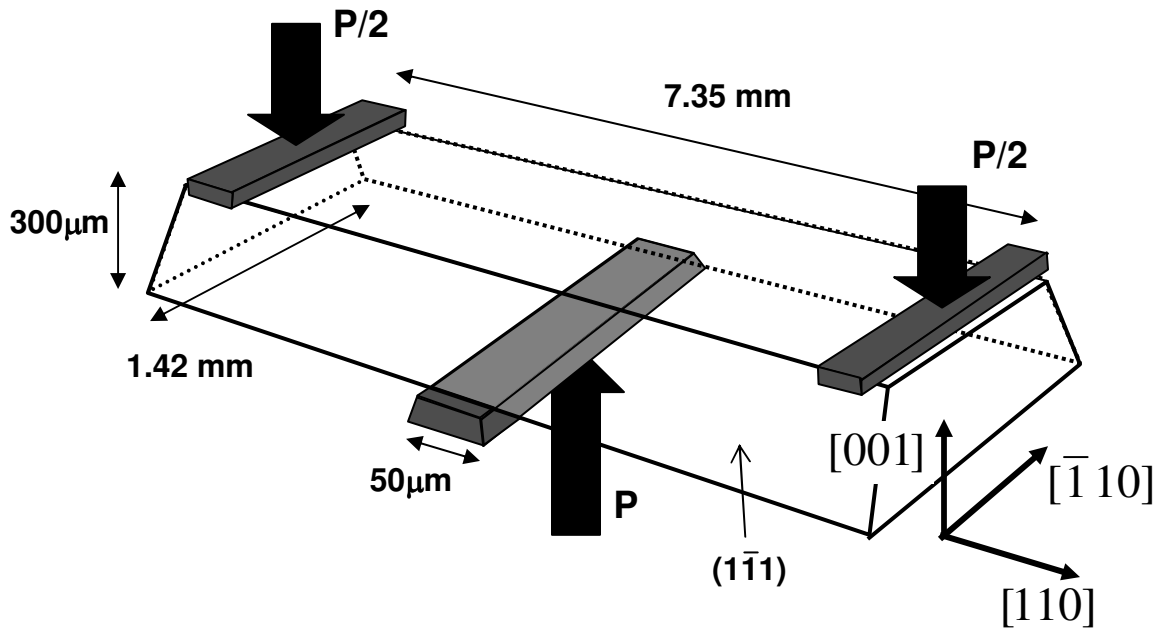

Figure 2: Geometry and crystallographic orientation of silicon three-point bend specimens used by Folk (2000) for brittle-ductile transition experiments.

Fig. 2

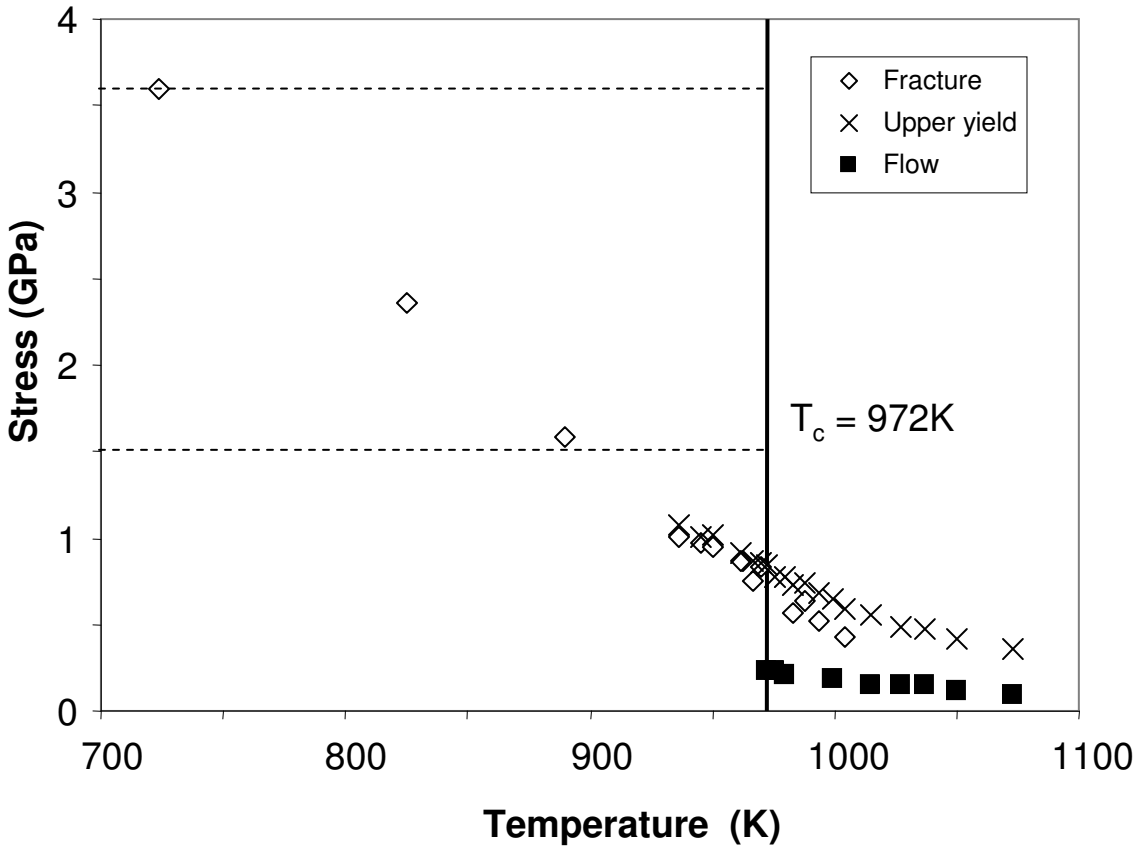

Figure 3: Typical experimental results (Folk 2000); fracture, upper yield and flow stresses as a function of test temperature for a strain rate of $6x10^{-5}$ s^{-1}. The dashed lines indicate the upper and lower limits of low temperature brittle fracture stresses.

Fig. 3

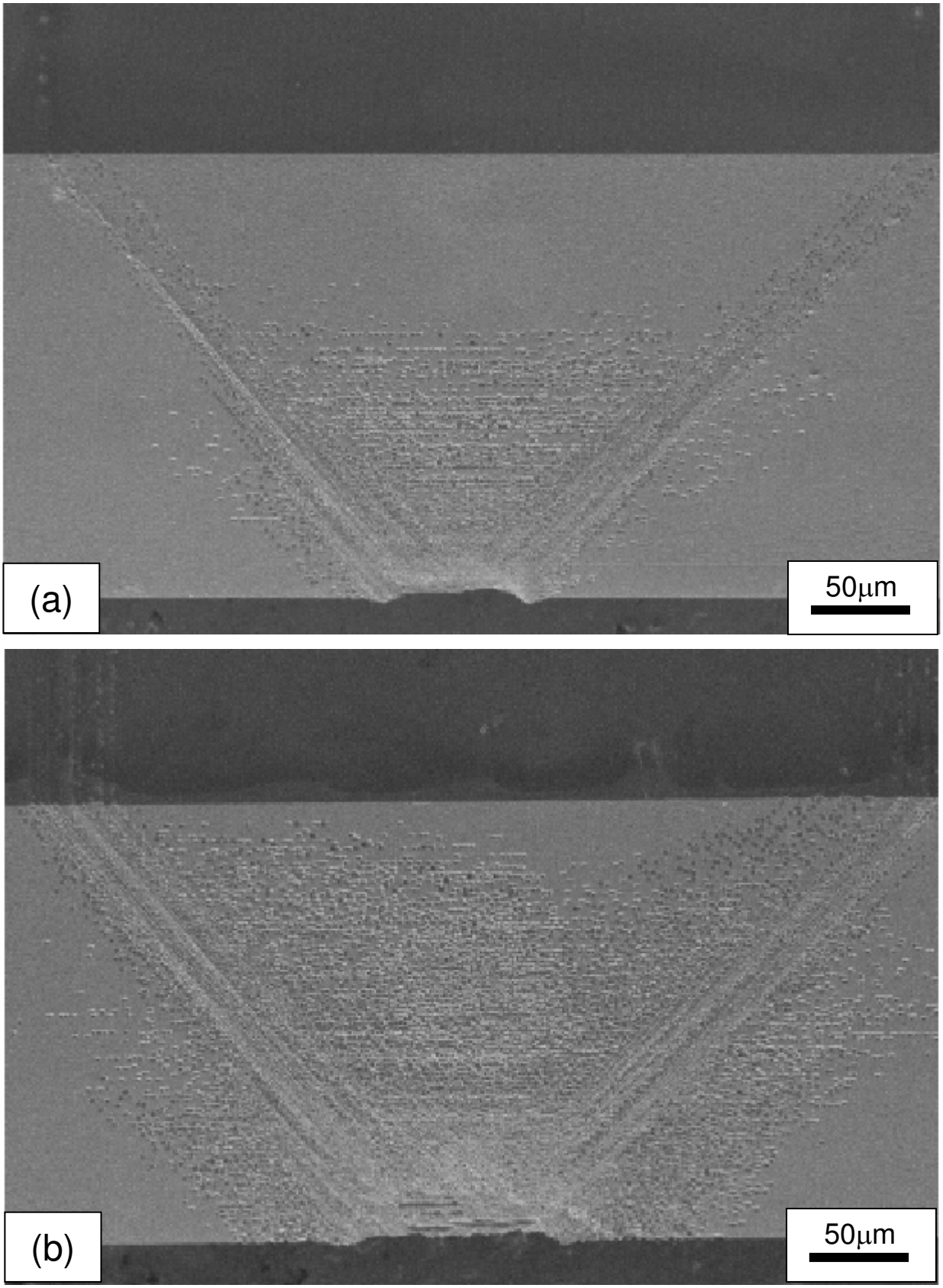

Figure 4: SEM micrographs of the etched inclined side and tensile faces of specimens loaded at 6 x 10^{-5} s^{-1} and 979K to (a) 60%, (b) 80% and (c) 100% of the peak stress, and (d) after the load drop. The central loading contact is on the bottom edge in each case.

Fig. 4

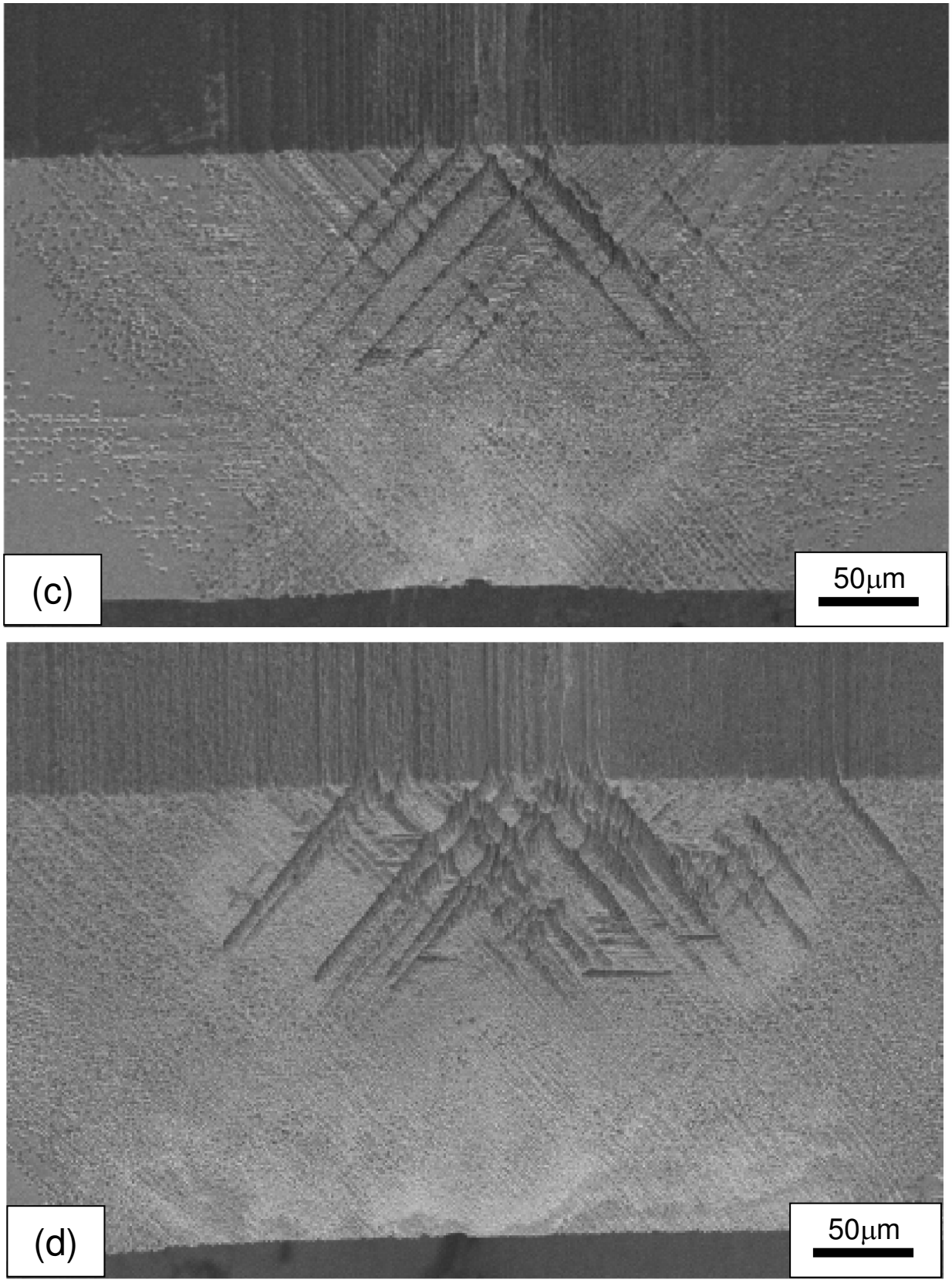

Figure 4: SEM micrographs of the etched inclined side and tensile faces of specimens loaded at 6 x 10^{-5} s^{-1} and 979K to (a) 60%, (b) 80% and (c) 100% of the peak stress, and (d) after the load drop. The central loading contact is on the bottom edge in each case.

Fig. 4

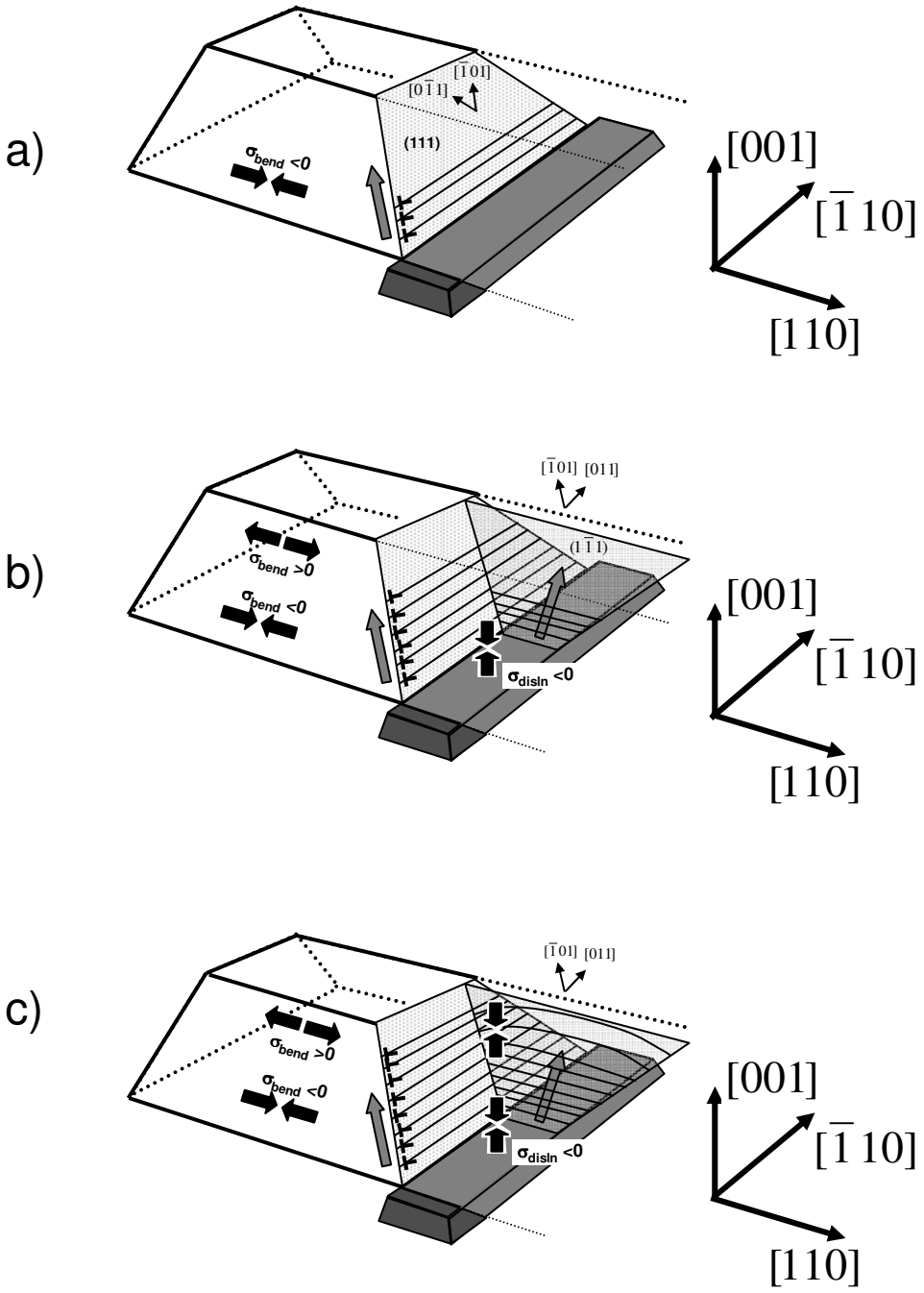

Figure 5: Proposed sequence of dislocation motion in the tests (see text): a) dislocations on type I slip systems nucleate at the contact edges and glide towards the tensile side of the specimen; b) secondary slip systems (type II) operate under the stresses from the contact and from dislocations on the primary systems; c) primary and secondary dislocations approach the tensile surface; d) secondary dislocation emerges at the tensile surface leaving a screw segment; e) screw segment cross-slips onto primary slip system forming a source near the tensile surface which can rapidly generate dislocations of type III; f) Dislocation types used in the model; co-ordinates used in equations (1) are also shown. For clarity, in (a)-(e), only one geometric variant of each slip system is shown, and the junctions between dislocations on type II and type I systems which terminate the type II dislocations are not shown.

Fig. 5

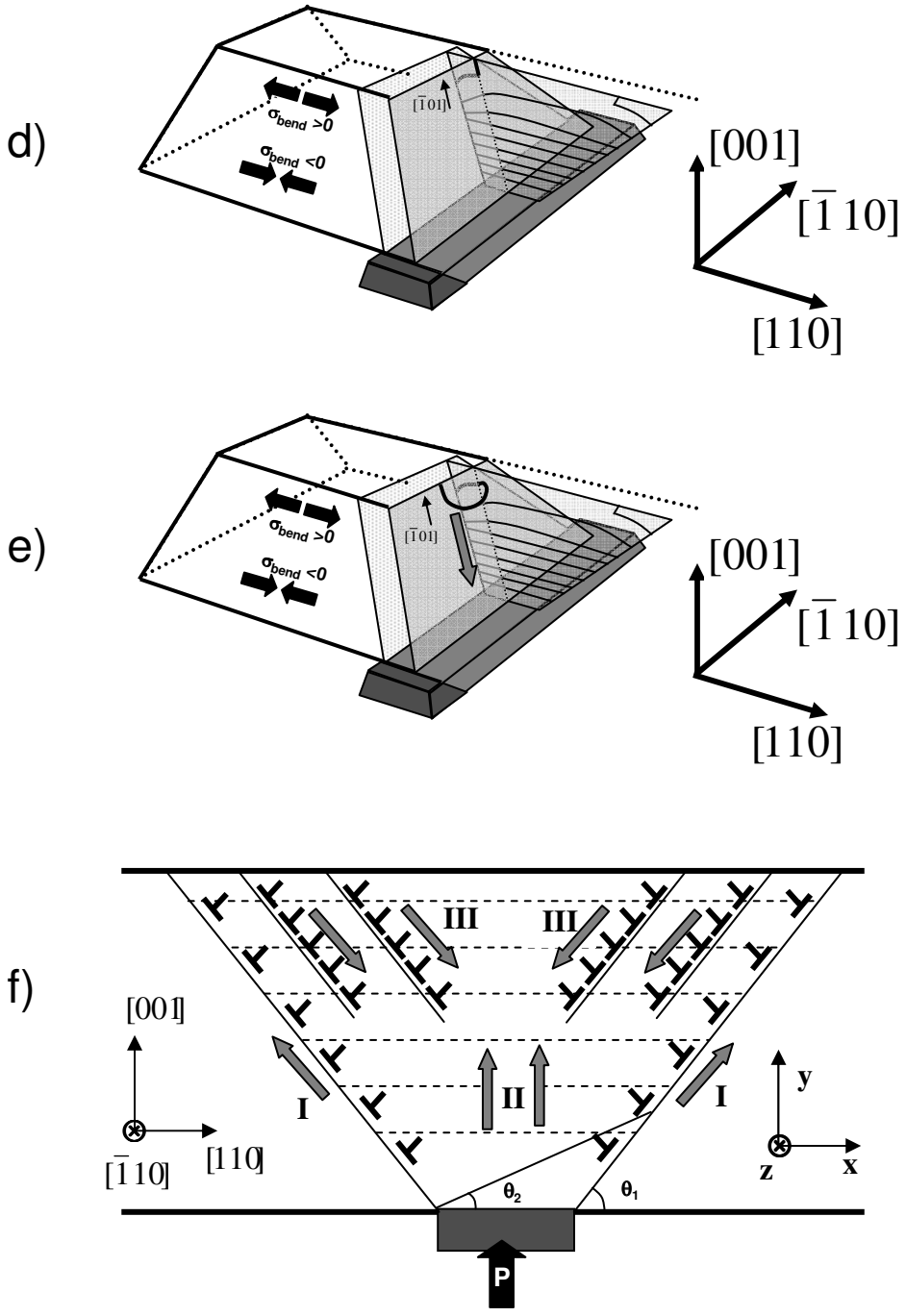

Figure 5: Proposed sequence of dislocation motion in the tests (see text): a) dislocations on type I slip systems nucleate at the contact edges and glide towards the tensile side of the specimen; b) secondary slip systems (type II) operate under the stresses from the contact and from dislocations on the primary systems; c) primary and secondary dislocations approach the tensile surface; d) secondary dislocation emerges at the tensile surface leaving a screw segment; e) screw segment cross-slips onto primary slip system forming a source near the tensile surface which can rapidly generate dislocations of type III; f) Dislocation types used in the model; co-ordinates used in equations (1) are also shown. For clarity, in (a)-(e), only one geometric variant of each slip system is shown, and the junctions between dislocations on type II and type I systems which terminate the type II dislocations are not shown.

Fig. 5

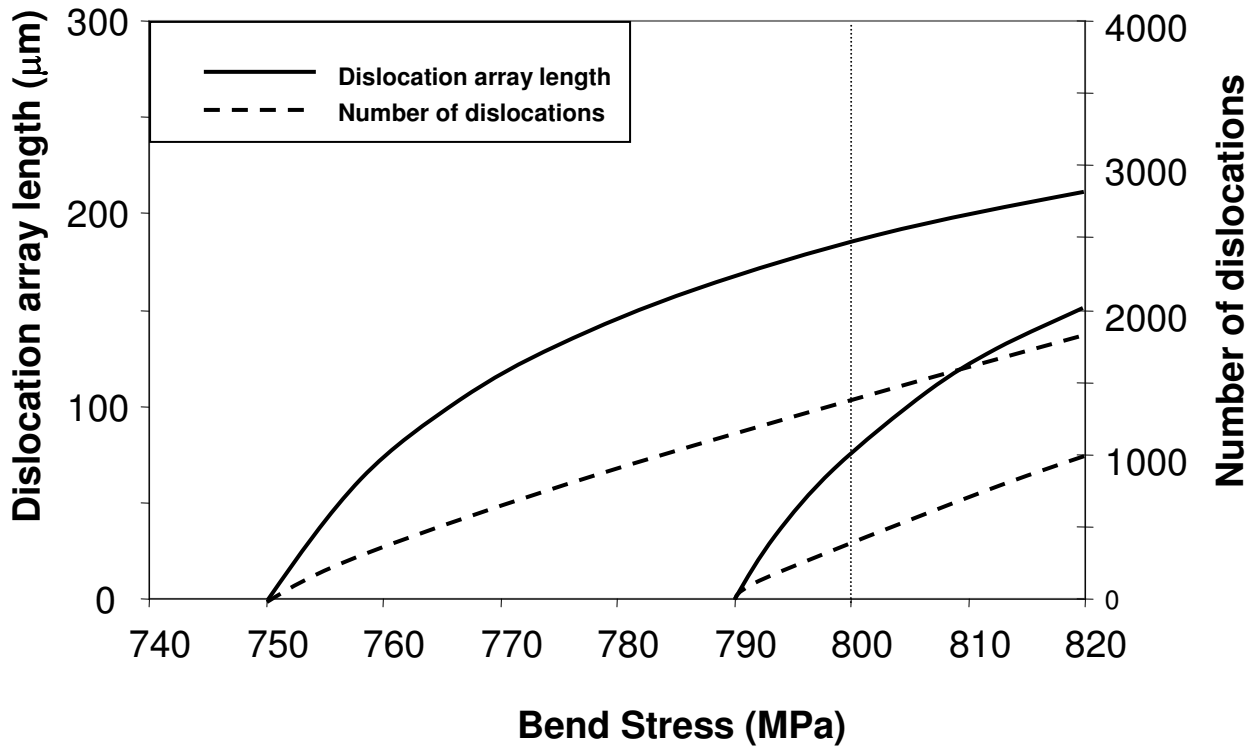

Figure 6: Modelling of type III dislocation arrays, nucleated at the tensile surface at two levels of bend stress (750 and 790 MPa).
Strain rate = $6x10^{-5}s^{-1}$, temperature = T_c for this strain rate = 972K. Fracture stress at the BDT is ~800 MPa (vertical dotted line).

Fig. 6

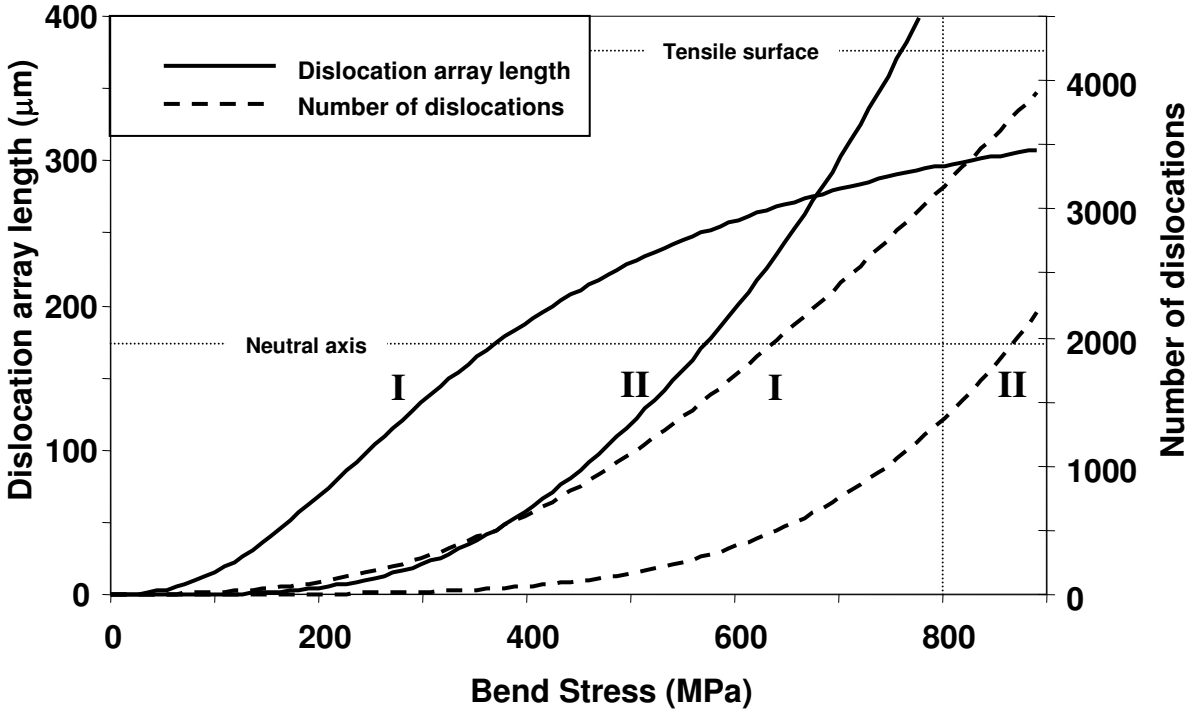

Figure 7: Modelling of types I and II dislocation arrays. Strain rate = $6x10^{-5}s^{-1}$, temperature = T_c for this strain rate = 972K. Fracture stress at the BDT is ~800 MPa (vertical dotted line). Horizontal dotted lines indicate the dislocation array lengths corresponding to the specimen's neutral axis and tensile surface.

Fig. 7

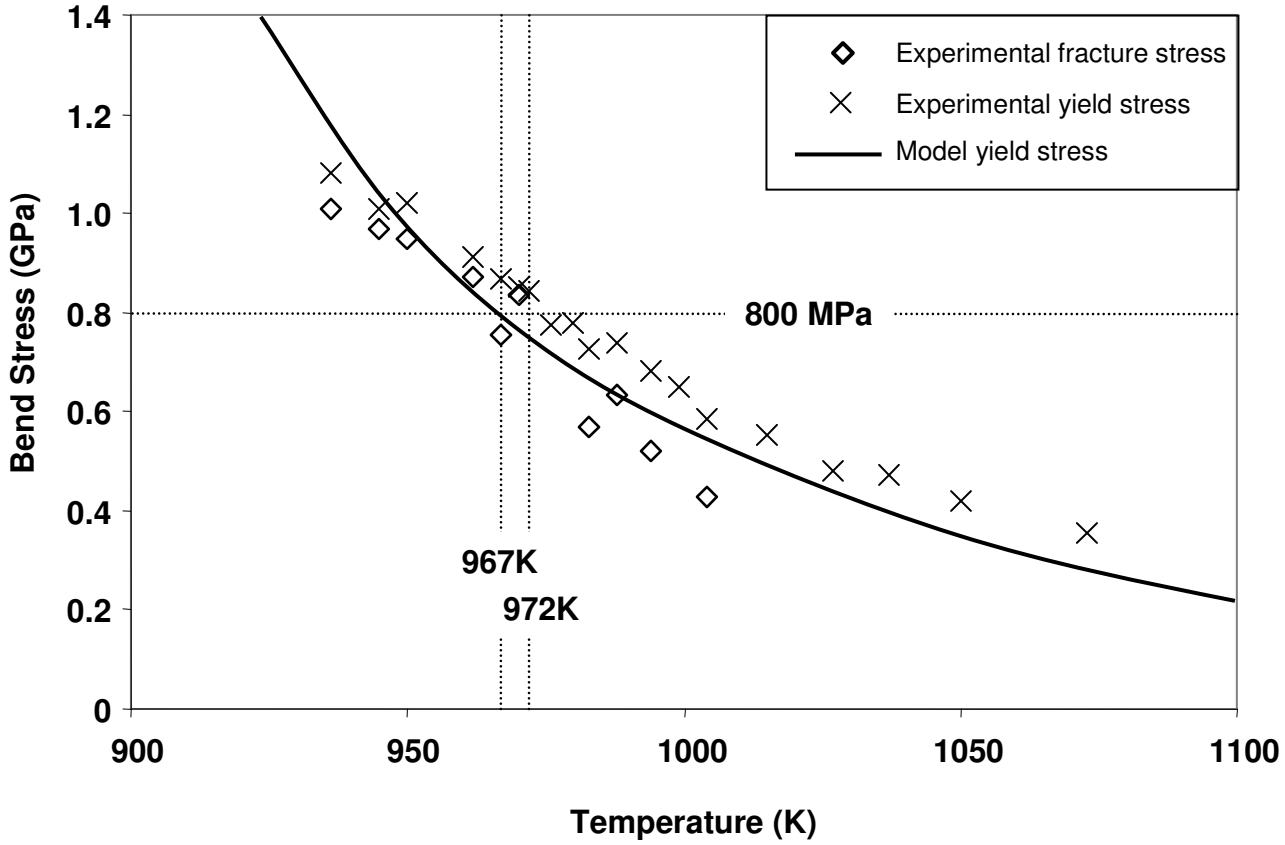

Figure 8: Temperature dependence of experimental fracture stress and experimental and modelled yield stress at a strain rate of 6 x 10^{-5} s^{-1}. The horizontal dotted line indicates the average experimental fracture stress at the brittle-ductile transition (800MPa); vertical lines indicate the experimental T_c (972 K) and the modelled T_c, where the modelled yield stress equals 800MPa (967K).

Fig. 8

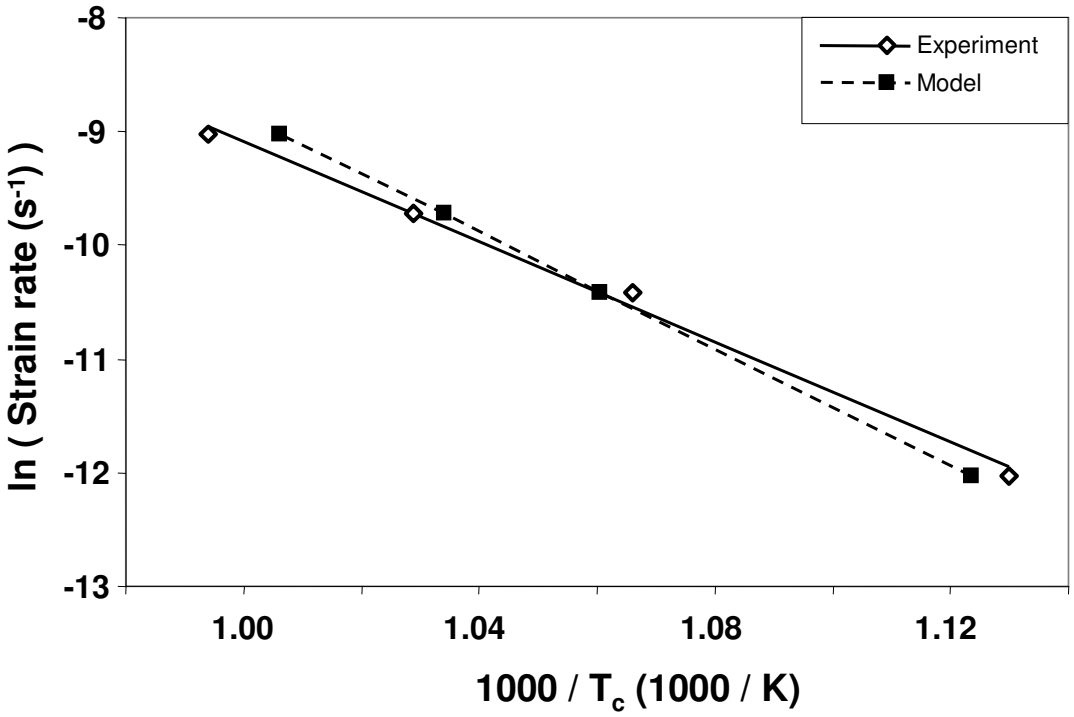

Figure 9: Arrhenius plots of strain-rate dependence of experimental and modelled brittle ductile transition temperatures (T_c). Activation energies corresponding to the best-fit lines are 1.9 eV for the experimental data and 2.2 eV for the model.

Fig. 9

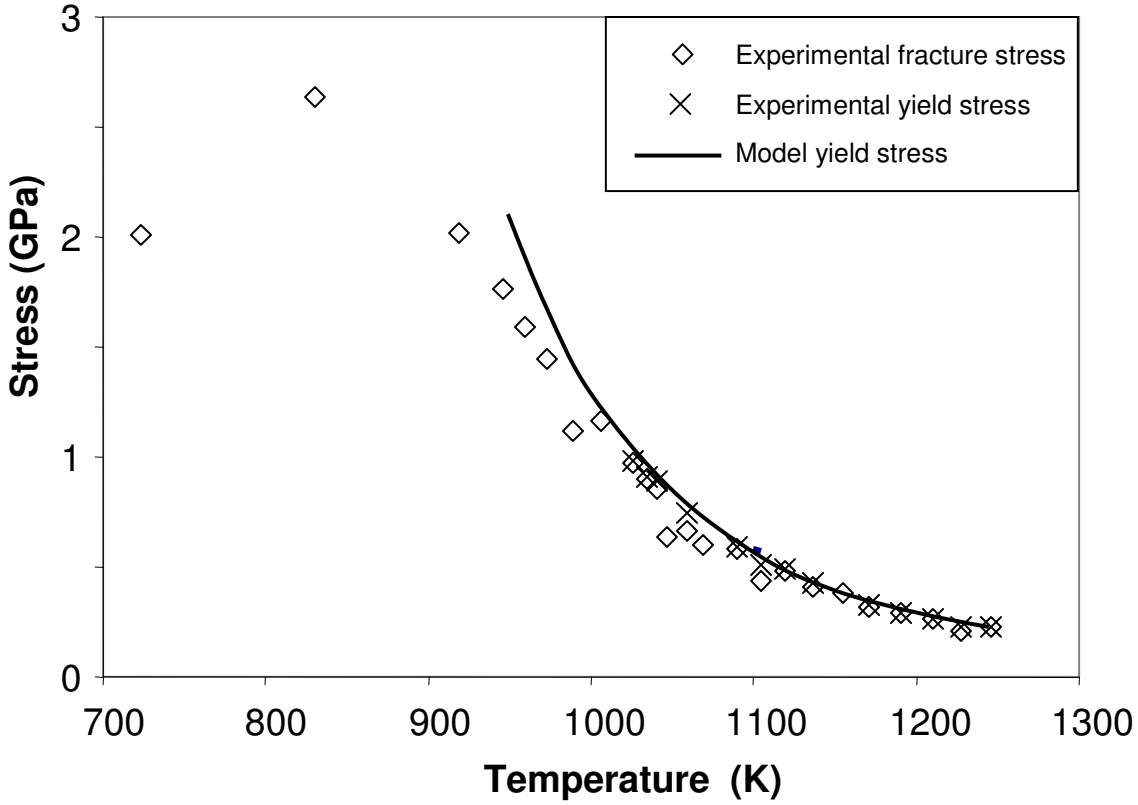

Figure 10: Experimental results (Folk 2000) for a strain rate of $6x10^{-4}$ s^{-1}; fracture and upper yield as a function of test temperature. The results of the model for upper yield stress (σ_N) for the same conditions are also shown..

Fig. 10